Pure Appl. Chem., Vol. 83, No. 4, pp. 885–898, 2011.
doi:10.1351/PAC-CON-10-09-24

Metal nanoparticle-enhanced radiative transitions: Giving singlet oxygen emission a boost*

Rasmus Toftegaard[1], Jacob Arnbjerg[1], Huaiping Cong[1], Hossein Agheli[2], Duncan S. Sutherland[3], and Peter R. Ogilby[1,‡]

[1]Center for Oxygen Microscopy and Imaging (COMI), Department of Chemistry, Aarhus University, Langelandsgade 140, 8000 Århus C, Denmark; [2]Applied Physics, Chalmers University of Technology, 412 96 Göteborg, Sweden; [3]Interdisciplinary Nanoscience Center (iNANO), Aarhus University, Ny Munkegade 120, 8000 Århus C, Denmark

Abstract: The fabrication and use of metal nanoparticles to influence electronic transitions in a given molecule is of growing interest; there is much to be gained by developing and exploiting methods to enhance weak optical signals. Singlet molecular oxygen, $O_2(a^1\Delta_g)$, which is an important intermediate in many oxidation reactions, particularly in biological systems, is ideally monitored by the 1275-nm $O_2(a^1\Delta_g) \rightarrow O_2(X^3\Sigma_g^-)$ phosphorescent transition. Unfortunately, the latter is highly forbidden and, as such, often presents a severe limitation in the application of this optical probe. In this paper, we describe how this weak phosphorescent transition can be enhanced by using localized surface plasmons (LSPs) from specially engineered gold nanostructures. In an attempt to elucidate the mechanism of this process, data were recorded from samples in which we decoupled the component of the plasmon resonance that absorbs incident light from the component that scatters incident light. We find that the latter appears to be the feature of significance in the process through which singlet oxygen phosphorescence is enhanced. In this work, we also illustrate how the singlet oxygen system provides an ideal model for a general study of metal-enhanced radiative rate constants.

Keywords: gold nanoparticles; metal-enhanced fluorescence; radiative transition; singlet oxygen; surface plasmon.

INTRODUCTION

Interest in the synthesis and characterization of metal nanoparticles has increased tremendously with the realization that such particles have unique properties that (i) challenge our understanding and interpretation of fundamental scientific principles, and (ii) have pertinent applications in a number of fields [1–3]. The characteristic feature of a metal nanoparticle that defines many properties of interest is the localized surface plasmon (LSP). The LSP reflects the confined motion of the electrons on the surface of the metal and, as such, depends on the material, size, and shape of the nanoparticle. Given the nanoparticle dimensions generally involved, these motions define an electric field that is pertinent with

*Paper based on a presentation made at the XXIII[rd] IUPAC Symposium on Photochemistry, Ferrara, Italy, 11–16 July 2010. Other presentations are published in this issue, pp. 733–930.

‡Corresponding author: E-mail: progilby@chem.au.dk.

respect to the interaction of the nanoparticle with visible and near-IR electromagnetic radiation [2,4–6]. As has been exemplified in recent years with gold and silver particles in particular, these nanomaterials can be useful in a range of applications that involve light, ranging from communications and imaging procedures to the development of new medical techniques [7–12].

The research community has increasingly focused on efforts to use metal nanoparticles to enhance electronic transitions in a molecule placed within the electric field defined by the LSP [13–16]. Although the development of a viable application-driven tool provides the impetus for many programs, a significant effort is also being devoted to elucidate the mechanism by which the LSP-dependent field can influence an electronic transition. In connection with our research program on singlet oxygen [17], we are likewise interested in specific features of an LSP.

Singlet oxygen, $O_2(a^1\Delta_g)$, the lowest-lying excited electronic state of molecular oxygen, is a reactive species with a rich and unique behavior pertinent to a wide range of scientific disciplines [17]. It is important in processes that include the degradation of polymeric materials and mechanisms by which cellular function is altered in both plant and animal systems. Indeed, singlet oxygen is a key intermediate in events that can result in cell death which, in turn, is the basis for the medical treatment of photodynamic therapy (PDT) where undesired tissue can be destroyed. With these points in mind, it becomes apparent that methods by which singlet oxygen can be monitored in a given system become important.

Over the past 30 years, the technique of choice to monitor singlet oxygen from a wide range of systems has invariably been the use of the 1275 nm $O_2(a^1\Delta_g) \rightarrow O_2(X^3\Sigma_g^-)$ phosphorescent transition [17–19]. This tool has recently been extended to also include microscope-based techniques where data can be recorded, for example, from a single biological cell [17,20,21]. Use of this phosphorescence as a probe, however, is limited by the fact that this transition is inherently very weak. From the perspective of selection rules defined by quantum mechanical principles, it is forbidden as an electric dipole process on the basis of electron spin, orbital angular momentum, symmetry, and parity. Indeed, even when perturbed by collisions with surrounding solvent, typical quantum yields of phosphorescence fall in the range of 10^{-5}–10^{-8} [18,19]. Although advances in instrumentation for detecting weak optical signals may eventually help alleviate some limitations associated with the use of this phosphorescence as a probe, it is clear that mechanisms by which one might enhance the $O_2(a^1\Delta_g) \rightarrow O_2(X^3\Sigma_g^-)$ transition could also have a significant impact. It is in this regard that we consider the effects of an electric field defined by the LSP of a metal nanoparticle.

The metal-enhanced phenomenon

It is well established that electric fields associated with specific metal surfaces can enhance a spectroscopic transition in a nearby molecule. The classic example of this phenomenon is surface-enhanced Raman scattering (SERS) [22]. It has likewise long been known that metal surfaces can enhance the intensity of IR absorption bands [23]. The related concept that a metal surface can influence the probability of an electronic transition has likewise been established [13–16], although much about this latter phenomenon remains to be understood and ultimately exploited [24,25]. To this end, the advent of techniques by which homogeneous distributions of metal nanoparticles with characteristic LSPs can be prepared is seen to be a boon [26–29].

Optical properties of nanostructures

The metal-enhanced phenomena in which we are interested are linked to the electronic and optical properties of the given nanoparticle being used. In short, aspects of the LSP are manifested in the optical properties of the particle (or a collection of such particles).

The observation that dispersions of small metal particles (i.e., colloids) give rise to distinct colors dates back to the fourth century [30]. However, the understanding of the physics behind this observation was not established until Mie solved the Maxwell equations for a spherical particle [31].

A plasmon is the quantum of energy related to the collective oscillation of electrons in a metal, and a surface plasmon derives from electron oscillation at the surface of the metal. When a large surface is divided into smaller parts, or when one constructs a nanoparticle, a confinement condition arises, and the resulting surface plasmon is then called a LSP. As we have mentioned, the LSP energy depends on the shape and size of the confined domain. A surface plasmon can be excited when the incident energy (e.g., light) is resonant with the energy of the plasmon, and this defines the localized surface plasmon resonance (LSPR). The LSPRs of easily prepared gold and silver spherical nanoparticles appear in the visible region of the spectrum, thus giving rise to the metal-dependent colors that have been known for centuries.

Due to the high symmetry of a spherical particle, the associated LSP is not easily tuned over a wide energy range. However, an asymmetric particle, such as a nanorod, exhibits transverse as well as longitudinal surface plasmon bands, both of which likewise respond to the particle geometry [29]. This increase in structural complexity makes it correspondingly easier to achieve LSPs over a wide range of energies. Recent advances in the development of methods by which asymmetric nanoparticles can be prepared in a controlled fashion have made it possible to correlate experimental LSPR data with theoretical predictions, thus adding further insight into our general understanding of the interaction between light and matter [5,28,29,32–35].

Metal-enhanced fluorescence and phosphorescence

With the advent of techniques by which novel nanoparticles can be prepared and characterized, it has become feasible to systematically address how such nanoparticles can perturb electronic transitions in a nearby molecule [13–16,36]. Because LSPRs in readily prepared gold and silver particles are in the visible region of the spectrum, much of the work thus far has focused on studying fluorescence and phosphorescence from common organic chromophores [13,37–41]. Enhancement has also been observed using other metals [42] as well as hybrid systems (e.g., metal-silica composites) [43]. In general, substantive evidence has been presented to support the fact that either fluorescence or phosphorescence can indeed be enhanced by placing the organic chromophore in a spatial domain near a metallic nanoparticle where the electric field is comparatively intense.

Scattering vs. absorption

To observe an LSP-dependent metal-enhanced effect on the emission from a given molecule, or more specifically on the radiative rate constant for emission, the energy of the transition being investigated must match that of the LSP. In short, a resonant condition must be achieved [44]. For a given particle, or ensemble of particles, the LSPR is readily ascertained by recording the extinction spectrum.

For light at a given frequency, ω, incident on a nanoparticle sample, the total extinction (E) due to the LSPR is given as the sum of the components for light scattering (S) and absorption (A). This relation can be expressed via the respective cross sections, σ, that are given in the Mie limit by eqs. 1–3 [45]

$$\sigma_{\mathrm{E}}(\omega) = \sigma_{\mathrm{A}}(\omega) + \sigma_{\mathrm{S}}(\omega) \tag{1}$$

$$\sigma_{\mathrm{A}}(\omega) = k\,\mathrm{Im}\left[\alpha'(\omega)\right] \tag{2}$$

$$\sigma_{\mathrm{S}}(\omega) = \frac{k^4}{6\pi}\left|\alpha'(\omega)\right|^2 \tag{3}$$

Here α' is a dipolar polarizability, modified with a retardation correction to account for finite wavelength effects, and k is the wave vector of the incoming light. Knowing the scattering-to-absorp-

tion ratio is fundamentally important as some theoretical considerations point to the fact that only the scattering properties of the nanostructures are relevant with respect to the radiative enhancement phenomenon [46,47]. Indeed, experiments described below have been performed with this in mind. Despite this statement about the scattering cross-section, the mechanism by which metal-enhanced luminescence occurs is still not fully understood. As outlined in this paper, we believe a study of the singlet oxygen system provides insight in this regard.

Singlet oxygen

It has already been established that, with appropriate control of the shape and size of a given nanoparticle, one can create an LSP that is energetically resonant with the 1275 nm $O_2(a^1\Delta_g) \rightarrow O_2(X^3\Sigma_g^-)$ transition [14,48]. Moreover, and arguably most importantly, we have also performed the proof-of-principle experiment demonstrating that the $O_2(a^1\Delta_g) \rightarrow O_2(X^3\Sigma_g^-)$ transition can indeed be enhanced by a nanoparticle with such an energetically matched LSP [14]. In the present paper, we discuss this phenomenon further, presenting new data pertinent for our attempt to elucidate mechanistic aspects of this metal-enhanced process.

A convenient method for singlet oxygen production, and the method employed in the present study, is photosensitization (Fig. 1) [17,18]. In this process, a molecule called the sensitizer (typically a large organic molecule), absorbs light in the UV–vis region of the spectrum to populate an excited singlet state, S_n. Fast internal conversion (k_{ic}) to the first excited singlet state, S_1, then occurs. For a good singlet oxygen sensitizer, this is followed by efficient intersystem crossing (k_{isc}) to the lowest-lying triplet state, T_1. This latter process kinetically competes with fluorescence from S_1. The lifetime of the T_1 state is usually sufficiently long for ground-state molecular oxygen to approach the sensitizer such that singlet oxygen can be created via collision-dependent energy transfer. The efficiency of this series of events is expressed through the singlet oxygen quantum yield, Φ_Δ, for a given sensitizer.

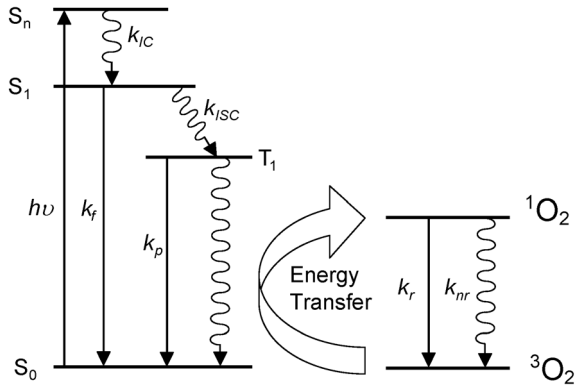

Fig. 1 Jablonski diagram showing the photosensitized production of singlet oxygen. The rate constants k_f and k_p refer to sensitizer fluorescence and phosphorescence, respectively.

The removal of the singlet oxygen thus produced can be described in terms of three general kinetically competing processes [17,18]: (1) Chemical reaction with a solute that might be present in the system. Such reactions are important in processes that result in the death of a biological cell, for example. (2) Interaction with a solute and/or the solvent that results in the nonradiative physical deactivation, or quenching, of singlet oxygen to regenerate the ground triplet state of oxygen (k_{nr} in Fig. 1). In our present experiments, the metal nanoparticle itself could quench singlet oxygen in this way. (3) Interaction with a solute and/or the solvent that results in the radiative deactivation of singlet oxygen to regenerate

the ground triplet state of oxygen (k_r in Fig. 1). It is this process with which we are arguably most interested in the present study. For the moment, it is important to recognize that the magnitude of k_r depends significantly on the molecule with which singlet oxygen collides [18,19,49,50]. Nevertheless, despite pronounced solvent effects on both k_{nr} and k_r, the magnitude of the solvent-dependent k_{nr} is generally much larger than k_r, which yields a small quantum efficiency for singlet oxygen phosphorescence, Φ_P (eq. 4, where τ_Δ is the singlet oxygen lifetime) [17–19].

$$\Phi_P = \Phi_\Delta \tau_\Delta k_r = \Phi_\Delta \frac{k_r}{k_{nr} + k_r} \tag{4}$$

Metal-enhanced effects in systems involving singlet oxygen

With Fig. 1 and eq. 4 in mind, it is important to distinguish between the possible ways that a metal nanoparticle can influence the photosensitized singlet oxygen system. On one hand, it has been shown that a metal can influence the yield of singlet oxygen production, by influencing the yields of the sensitizer singlet and triplet excited states (i.e., influencing the yield of the singlet oxygen precursor) [51]. Although one must be aware that such a phenomenon can occur, one must also acknowledge that singlet oxygen production is rarely a limiting factor in many systems of practical importance; there are already a plethora of sensitizers that produce singlet oxygen with a quantum efficiency near unity.

On the other hand, the metal nanoparticle could influence the radiative rate constant for the $O_2(a^1\Delta_g) \rightarrow O_2(X^3\Sigma_g^-)$ transition and, by extension, the quantum efficiency of singlet oxygen phosphorescence. Because the latter is often a limiting factor in detecting singlet oxygen (i.e., $\Phi_P \sim 10^{-5}$–10^{-8}), any metal-enhanced gain here will be of great benefit.

RESULTS AND DISCUSSION

Optical properties of the gold nanodiscs

To successfully enhance the radiative transition from singlet oxygen to ground-state oxygen, one needs a metal nanostructure where the LSP is tuned to match the $O_2(a^1\Delta_g) \rightarrow O_2(X^3\Sigma_g^-)$ transition at 1275 nm. To this end, we opted to work with gold nanodiscs on a flat glass substrate (Fig. 2). Using a lithographic technique [32], one can readily prepare samples in which (1) the size of the disc is controlled and (2) all of the discs have the same size. Indeed, efforts to minimize the effects of polydispersity on the inhomogeneous broadening of the ensemble optical response is a key factor in ensuring that experiments can be performed in which more than one disc is sampled while still retaining a comparatively narrow LSPR spectral profile.

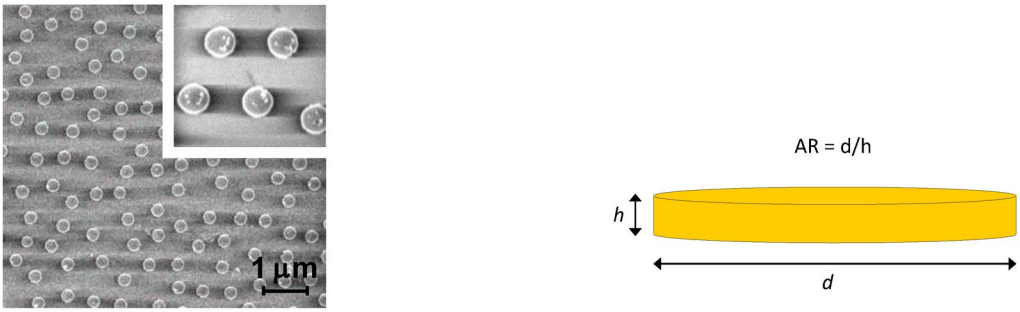

Fig. 2 (Left) SEM image of gold nanodiscs on a glass substrate. For this sample, the disc diameter, *d*, is ~260 nm and height, *h,* is ~20 nm. The inset shows the same discs but with a higher magnification. (Right) Illustration of one disc showing the aspect ratio, AR.

With these nanodiscs, the energy of the LSP is readily tuned by changing the diameter-to-height aspect ratio, AR, (Fig. 2). In short, with an increase in AR, the LSPR shifts to longer wavelengths. The exact spectral position of the LSPR also depends on the refractive index of the dielectric medium surrounding the nanodiscs (Fig. 3), and this must be taken into consideration when preparing the system designed to enhance the $O_2(a^1\Delta_g) \rightarrow O_2(X^3\Sigma_g^-)$ transition.

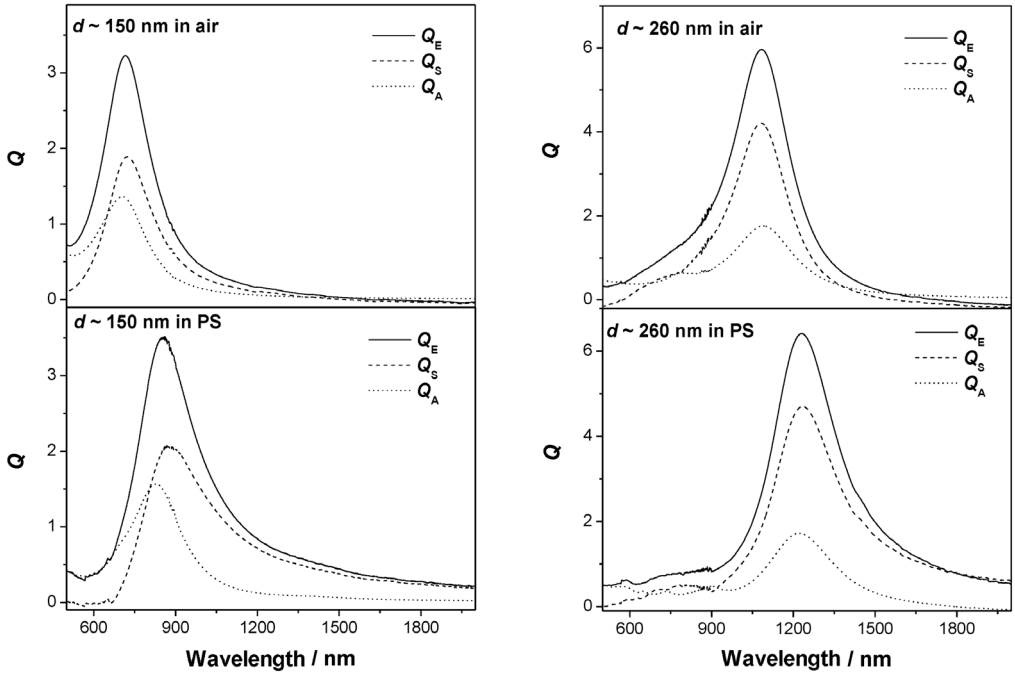

Fig. 3 Measured extinction, scattering and absorption efficiencies (Q_E, Q_S, and Q_A, respectively) for gold discs with d ~ 150 nm (left) and d ~ 260 nm (right). The efficiencies, Q, were obtained as the measured signal divided by the fractional area covered by the gold nanodiscs (22 and 11 % for the smaller and larger discs in the polystyrene (PS) matrix, respectively). The data show that the respective band maxima depend significantly on the medium in which the discs are embedded.

For our proof-of-principle experiments, two different disc samples were prepared: one with discs in which the LSPR has a maximum at a shorter wavelength than the 1275 nm $O_2(a^1\Delta_g) \rightarrow O_2(X^3\Sigma_g^-)$ transition (h ~ 20 nm, d ~ 150 nm) and another in which the LSPR is resonant with the 1275 nm $O_2(a^1\Delta_g) \rightarrow O_2(X^3\Sigma_g^-)$ transition (h ~ 20 nm, d ~ 260 nm) (Figs. 3,4). The SEM image shown in Fig. 2 illustrates another key aspect of our samples: in this case, the average disc density on the glass substrate is 2.2 discs/μm^2 and corresponds to a projected area coverage of 11 %. As such, the distance between discs is sufficiently large to preclude near-field coupling between the respective LSPs [14,52–55]. The distribution of the discs shows no long-range order which minimizes the effects of longer-range dipole coupling seen in regular array configurations [14].

In Fig. 3, we show representative extinction spectra for these two disc samples. Moreover, by independently recording the absorption spectra for these samples, we are able to isolate the scattering spectrum. Also shown in Fig. 3 are the effects of changing the refractive index of the surrounding medium. To make our samples easier to handle, we used glassy polystyrene (PS) as the solvent for the singlet oxygen experiment. As such, it was necessary to design the AR of the structures to ensure that,

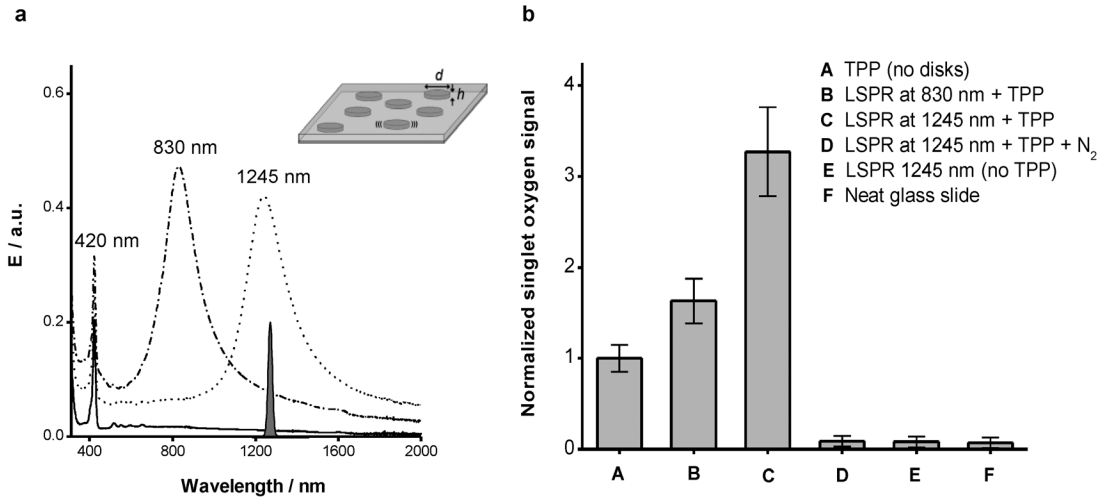

Fig. 4 (a) Extinction spectra of a sample with no discs (solid line), of a sample with discs with $d \sim 150$ nm (dashed-dot) and of a sample with discs with $d \sim 260$ nm (dotted). The peak maxima of the respective LSPR bands are shown. For all three samples, the 420-nm Soret band of the porphyrin used as a singlet oxygen sensitizer is clearly seen. The spectral profile of singlet oxygen phosphorescence is indicated by the curve shaded in gray. A schematic representation of the gold disc sample is shown as an inset. (b) Singlet oxygen signal magnitudes observed from various samples. All samples were in a ~100 nm thick PS matrix.

with the solvent-induced red-shift of the LSPR, we would indeed be resonant with the 1275 nm $O_2(a^1\Delta_g) \rightarrow O_2(X^3\Sigma_g^-)$ transition.

Enhancement of singlet oxygen phosphorescence

Parallel experiments were performed with samples that had no nanodiscs, nanodiscs with $d \sim 150$ nm in which the LSPR was not resonant with the $O_2(a^1\Delta_g) \rightarrow O_2(X^3\Sigma_g^-)$ transition, and nanodiscs with $d \sim 260$ nm in which the LSPR was resonant with the $O_2(a^1\Delta_g) \rightarrow O_2(X^3\Sigma_g^-)$ transition (Fig. 4a). All samples were coated with a thin layer (~100 nm) of PS doped with the singlet oxygen sensitizer tetraphenylporphyrin, TPP. The TPP concentrations employed were about 50 mM to yield absorbances of 0.2–0.3 at 420 nm, Fig. 4a.

Despite working with comparatively high TPP concentrations, evidence of aggregation was not observed in the TPP absorption or fluorescence spectra. The presence of TPP was evident, however, when examining the kinetics of singlet oxygen decay in a time-resolved experiment [14]. The singlet oxygen lifetimes thus obtained, $\tau_\Delta = 16$–18 μs, were independent of whether the sample contained discs or not, and are consistent with a system in which there is moderate quenching of singlet oxygen by TPP [56]. Also, the spectral profile of the emission signal recorded was identical in all samples and, with the spectral resolution limited by the use of a series of interference filters, was consistent with that expected for the $O_2(a^1\Delta_g) \rightarrow O_2(X^3\Sigma_g^-)$ transition.

The laser beam used to irradiate TPP at 420 nm was focused to a ~1.4-μm-diameter spot at the sample and thus covered 3.4–26 nanodiscs, depending on the sample and the disc density [14]. Upon irradiation at a given position on the sample, emission was independently monitored at three different wavelengths: 650 nm (TPP fluorescence), 1200 nm (background signal), and 1275 nm (singlet oxygen phosphorescence). Data recorded from several irradiation positions were averaged. The data obtained did not vary notably with the position on the sample that was irradiated, which is consistent with the fact that the samples appeared homogenous.

The data, normalized for differences in absorbance at the excitation wavelength, are shown in Fig. 4b. It is clear that the intensity of the singlet oxygen phosphorescence signal is much greater from the disc-containing sample in which the LSPR is resonant with the $O_2(a^1\Delta_g) \rightarrow O_2(X^3\Sigma_g^-)$ transition. For the disc-containing sample in which the LSPR is not resonant with the $O_2(a^1\Delta_g) \rightarrow O_2(X^3\Sigma_g^-)$ transition, the phosphorescence intensity observed is still greater than that observed in the disc-free control sample. This is reasonable considering that the "tail" of the LSPR in the non-resonant sample still has appreciable intensity at 1275 nm (Fig. 4a). Furthermore, we verified that no singlet oxygen phosphorescence was produced following 420 nm irradiation of (1) TPP in a sample in equilibrium with an oxygen-free atmosphere, (2) TPP-free gold nanodiscs, or (3) a neat glass slide (Fig. 4b).

Enhancement of the 650-nm TPP fluorescence was not observed in either disc-containing sample, indicating that the effect shown in Fig. 4b is not due to metal-enhanced absorption in the sensitizer or to lateral scattering of excitation light leading to artifacts of increased path length. Furthermore, we performed additional experiments using a microscope objective with a smaller numerical aperture. If lateral scattering in the disc sample was a problem, we would expect to see different enhancement factors (relative to a sample without discs) when using two different objectives because emitted light would then be collected from different solid angles. We observed no change in the enhancement factor when using different objectives; only the signal magnitude changed according to the different collection efficiencies. Experiments where the sample was tilted slightly with respect to the incoming laser beam likewise resulted in no changes in observed enhancement.

Returning to eq. 4, the absence in our samples of a metal-enhanced effect on TPP fluorescence implies that there is likewise no metal-enhanced effect on the quantum yield of singlet oxygen, Φ_Δ. This is arguably expected given the position of the LSPRs in our sample. In any event, even if there was an effect on Φ_Δ, because the inherent singlet oxygen yield for TPP is already high ($\Phi_\Delta = 0.7$) [57], a metal-enhanced increase in the production efficiency of singlet oxygen would not be able to account for the observed data. Moreover, we have also ascertained that the metal discs have no effect on the singlet oxygen lifetime, τ_Δ. Thus, the data are consistent with a plasmon-dependent increase in the rate constant for $O_2(a^1\Delta_g) \rightarrow O_2(X^3\Sigma_g^-)$ radiative decay, k_r, eq. 4. It is important to note that this increase in k_r is not manifested in the values of τ_Δ (vide supra) because, under all conditions, singlet oxygen decay is still dominated by nonradiative pathways (i.e., despite enhancing k_r, we still have $k_r << k_{nr}$ and $\tau_\Delta \approx {k_{nr}}^{-1}$).

The "true" enhancement factor

In considering the logistics of how our experiments were performed, it becomes clear that the "true" extent to which k_r is enhanced must be larger than the observed value of ~3.5 shown in Fig. 4b. The distance over which the plasmon-dependent electromagnetic field extends away from the nanodiscs is not large [58], and we estimate that the corresponding plasmon-influenced volume in our system is less than 1 % of the total volume containing the TPP that is irradiated. Thus, the number of singlet oxygen molecules that experience the effect of the LSP-dependent field is only a small fraction of the total number of singlet oxygen molecules produced and, by extension, detected in our experiment. In support of this statement we performed independent experiments with thicker PS films over the discs, keeping the TPP concentration fixed. In this case, as expected, the enhancement factor indeed decreased.

Thus, the enhancement of k_r for those molecules within the near-field of the LSP must be significantly greater than the average factor of ~3.5 measured [14]. Moreover, it should be possible to increase k_r to the extent where this radiative transition dominates singlet oxygen deactivation, (i.e., $k_r >> k_{nr}$) and thereby obtain phosphorescence yields close to unity (eq. 4). However, the experimental realization of this hypothetical situation will likely involve more sophisticated design of the nanoparticles as well as the experimental approach.

Nanosandwiches

The spectra shown in Fig. 3 indicate that the disc-containing samples from which enhanced singlet oxygen phosphorescence was observed have extinction spectra in which the LSPR is characterized by a comparatively large component of optical scattering as opposed to absorption. We have alluded to the fact that some theoretical treatments expect a correlation between the scattering cross-section and the propensity of a given metal particle to enhance a radiative process [15]. In an attempt to experimentally address this fundamental question, we set out to prepare and use nanoparticles in which we could control the relative magnitudes of the scattering and absorption cross-sections.

We felt that the most reasonable approach to this end would be to exploit hybridization effects associated with the coupling of LSPs from separate, but adjacent, nanoparticles. As such, we extended our disc structures and constructed "nanosandwiches", Fig. 5, in which a dielectric silica disc is sandwiched between two gold discs [59].

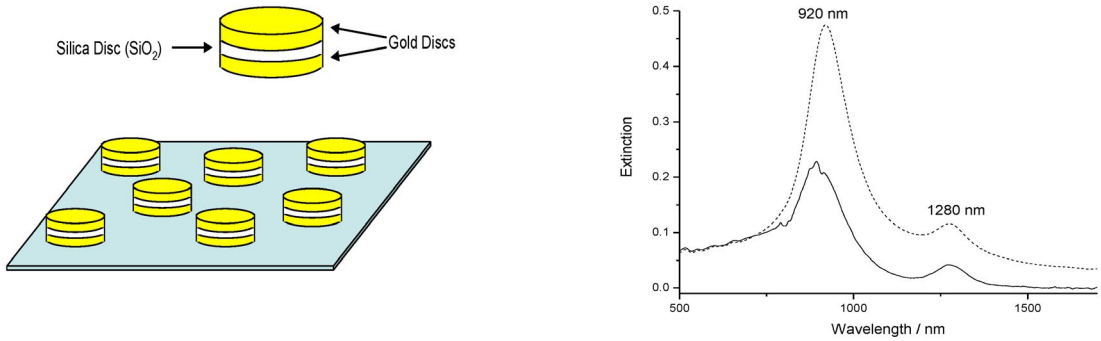

Fig. 5 (Left) Illustration of the "nanosandwiches" in which a silica disc is sandwiched between two gold discs. (Right) Extinction spectra (dashed line) and absorption (solid line) recorded from such nanosandwiches with a diameter of 190 nm and in which the gold layers were 22 nm thick and the silica layer was 11 nm thick. The spectra were recorded from samples embedded in PS.

For the current discussion we note that this sandwich geometry gives rise to hybridization between LSPs on the two discs that produce distinct resonances in the extinction spectrum (Fig. 5). For our particular sample, the more intense resonance with a band maximum at ~920 nm is composed of both scattering and absorption components, just as in the single disc structure (Fig. 3). However, for the sandwich with this geometry, we are also able to obtain an LSPR that is energetically close to the $O_2(a^1\Delta_g) \rightarrow O_2(X^3\Sigma_g^-)$ transition (Fig. 5). Although not particularly intense, this band with a maximum at ~1280 nm is the result of asymmetric LSP coupling, and the spectral feature is predominantly due to light absorption (admittedly, this absorption band sits on a featureless tail of the scattering component whose band maximum is at ~920 nm). As such, when using this sandwich in a singlet oxygen experiment, we might not expect to see an enhanced phosphorescence signal. Upon performing the experiment, and within our detection error, there was indeed no evidence of a metal enhanced effect on the $O_2(a^1\Delta_g) \rightarrow O_2(X^3\Sigma_g^-)$ transition.

Solution-phase experiments

Although the use of nanodiscs immobilized on a glass substrate has many advantages in a mechanistic study of metal-enhanced radiative transitions, it also has limitations. For a number of reasons, including ease of preparation and practical applications, it would be of benefit to develop a technique whereby suitable nanoparticles could be prepared and used in bulk solution-phase experiments.

In recent years, there has been a considerable effort to prepare asymmetrical nanoparticles that can be suspended in solution and whose LSPRs can be tuned over a wide range of the spectrum, including the near-IR in a domain spectrally coincident with the $O_2(a^1\Delta_g) \rightarrow O_2(X^3\Sigma_g^-)$ transition [48]. When considering the data obtained thus far in terms of our own desires, we wanted to avoid an approach that was based on a simple nanostructure (i.e., a gold nanorod) because, with the ARs required to obtain an LSPR at 1275 nm, rather complicated synthetic, purification, and handling procedures would be needed to ensure the production of a homogeneous distribution of particles that did not aggregate. Rather, we opted to focus on the preparation of composite particles that take advantage of the interaction between different gold layers. As outlined in our discussion on the nanosandwiches, this approach would, in principle, also allow us to discriminate between the scattering and absorption cross sections.

With these points in mind, we first used convenient and well-established chemistry to prepare gold nanorods with a comparatively small AR (i.e., the LSPR is in the visible region of the spectrum, at an energy much higher than that of the $O_2(a^1\Delta_g) \rightarrow O_2(X^3\Sigma_g^-)$ transition). We then coated these nanorods with a layer of silica, onto which we finally added an overcoat of gold to create a "nanorod-in-nanoshell" geometry. These steps are illustrated in Fig. 6.

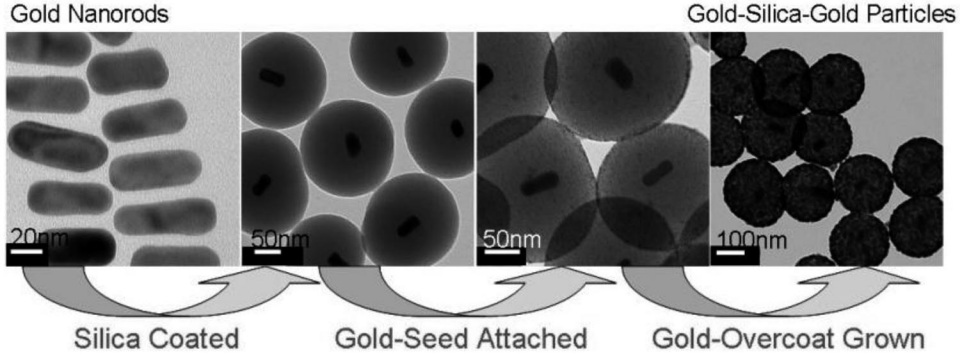

Fig. 6 Illustration of the steps involved in the preparation of a gold-silica-gold multilaminate particle with appreciable extinction at 1275 nm [48].

Gold nanoshells have previously been shown to exhibit resonances in the near-IR [60]. As mentioned, however, we wanted to capitalize on potentially helpful effects of hybridization between the nanoshell LSP modes and the nanorod LSP modes. We ascertained that, as expected, changes in the dimensions of any one of these layers indeed result in a change in the spectroscopic properties of the nanoparticles [48].

Most importantly, these multilayer nanoparticles yield a LSPR with appreciable extinction at 1275 nm (Fig. 7) [48]. The fact that this LSPR band is quite broad likely reflects, in part, the asymmetry of the coupling between the core gold nanorod and the gold overcoat (i.e., the distance between the core rod and the outer layer varies given the asymmetry of the rod).

From the extinction spectrum shown in Fig. 7, it would appear that our multilaminate gold-silica-gold particles are well suited to enhance singlet oxygen phosphorescence. Unfortunately, at the desired wavelength of 1275 nm, the optical extinction is mainly of an absorbing nature. In this way, our multilaminate particles resemble the nanosandwiches. Indeed, when recording singlet oxygen phosphorescence intensities, there was no evidence of a metal-dependent enhancement with these multilaminate particles. This is an effective reminder that achieving the appropriate LSPR in a metal nanoparticle is not enough; it appears that the LSPR must also be based on a large scattering cross-section.

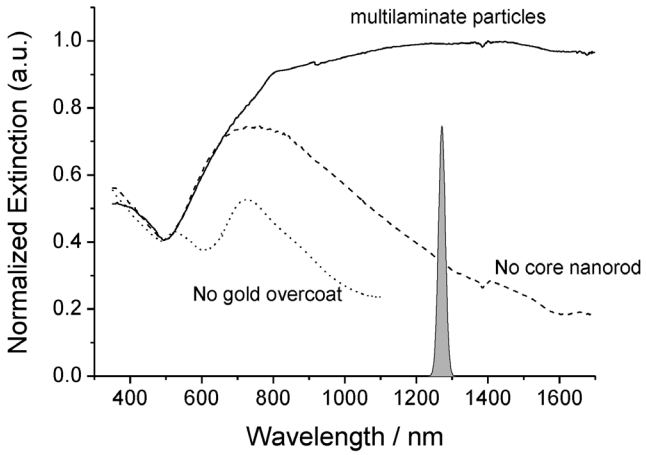

Fig. 7 Normalized extinction spectra of a dilute aqueous dispersion of multilaminate silica-coated gold nanorods with a gold overcoat (solid line). These data were obtained from 20 × 60 nm nanorods with a silica shell ~60 nm thick and a ~15-nm gold overcoat. Also shown are the extinction spectra recorded from (a) identical gold-coated silica particles that lack the core gold nanorod (dashed line) and (b) identical silica-coated gold nanorods that lack the gold overcoat (dotted line). The spectral profile of singlet oxygen phosphorescence is indicated by the curve shaded in gray.

Mechanistic aspects of the enhanced $O_2(a^1\Delta_g) \rightarrow O_2(X^3\Sigma_g^-)$ radiative transition

We have demonstrated that the LSP associated with a metal nanoparticle can be used to enhance the $O_2(a^1\Delta_g) \rightarrow O_2(X^3\Sigma_g^-)$ radiative transition. One advantage of using this singlet oxygen system as a model to study the perturbing effects that a metal might have on a radiative transition is the fact that a great effort has already been expended to examine the effect to which a given solvent molecule will influence the $O_2(a^1\Delta_g) \rightarrow O_2(X^3\Sigma_g^-)$ radiative transition [18,19,49,50,61–64].

It is established that the rate constant for $O_2(a^1\Delta_g) \rightarrow O_2(X^3\Sigma_g^-)$ phosphorescence is comparatively small, principally reflecting the fact that this process is highly forbidden as an electric dipole transition. It has also been established that, upon interaction with a perturbing molecule, (1) the magnitude of the $O_2(a^1\Delta_g) \rightarrow O_2(X^3\Sigma_g^-)$ radiative rate constant can increase appreciably and (2) the extent of this change increases with an increase in the polarizability of the perturbing molecule [49,63,64]. This phenomenon has been attributed to a perturbation-induced, symmetry-disrupting process whereby the $O_2(a^1\Delta_g) \rightarrow O_2(X^3\Sigma_g^-)$ radiative transition can steal intensity from more allowed transitions between other states in the oxygen molecule [50].

With this background in mind, it seems reasonable to suggest that the nanoparticle LSP may influence oxygen in the same way providing a perturbation that facilitates state mixing in oxygen and, as a consequence, making it possible for the $O_2(a^1\Delta_g) \rightarrow O_2(X^3\Sigma_g^-)$ transition to steal intensity from other more allowed transitions in the oxygen molecule. The foundation upon which the solvent-dependent perturbation of singlet oxygen is based is the notion that one is dealing with a "complex" between a given solvent molecule, M, and the oxygen molecule [65]. Indeed, this same notion of a "complex" has also been advocated by Lakowicz et al. to account for metal-enhanced fluorescence [15].

CONCLUSION AND OUTLOOK

We have established that the $O_2(a^1\Delta_g) \rightarrow O_2(X^3\Sigma_g^-)$ transition in oxygen provides an ideal and relevant system to study the effects of a metal nanoparticle on the rate constant for a radiative process. We have not only demonstrated that the $O_2(a^1\Delta_g) \rightarrow O_2(X^3\Sigma_g^-)$ phosphorescent transition can indeed be

enhanced by a metal nanoparticle with an appropriate LSPR, but that the efficiency of the enhancement phenomenon is likely to depend on an appreciable scattering component of the metal nanostructure.

As this field evolves, we expect much can be gained by the further development and implementation of techniques whereby nanoparticles with a large scattering cross-section can be readily made and functionalized. Indeed, by localizing a singlet oxygen sensitizer near the metal surface and, hence, by directly producing a large population of singlet oxygen in the electric field associated with the LSP, we anticipate that a comparatively large enhancement in the $O_2(a^1\Delta_g) \rightarrow O_2(X^3\Sigma_g^-)$ phosphorescence will ensue. In turn, this could be extremely useful in a number of applications, particularly with respect to the optical detection of singlet oxygen in single biological cells during studies of cell death mediated by singlet oxygen [17,20].

ACKNOWLEDGEMENTS

This work was supported by a grant from the Danish National Research Foundation.

REFERENCES

1. P. V. Kamat. *J. Phys. Chem. B* **106**, 7729 (2002).
2. M. A. El-Sayed. *Acc. Chem. Res.* **34**, 257 (2001).
3. R. W. Murray. *Chem. Rev.* **108**, 2688 (2008).
4. M. Kanehara, H. Koike, T. Yoshinaga, T. Teranishi. *J. Am. Chem. Soc.* **131**, 17736 (2009).
5. S. Link, M. A. El-Sayed. *J. Phys. Chem. B* **103**, 8410 (1999).
6. K. L. Kelly, E. Coronado, L. L. Zhao, G. C. Schatz. *J. Phys. Chem. B* **107**, 668 (2003).
7. P. K. Jain, X. H. Huang, I. H. El-Sayed, M. A. El-Sayed. *Plasmonics* **2**, 107 (2007).
8. C. Wu, X. Liang, H. Jiang. *Opt. Commun.* **253**, 214 (2005).
9. N. J. Durr, T. Larson, D. K. Smith, B. A. Korgel, K. Sokolov, A. Ben-Yakar. *Nano Lett.* **7**, 941 (2007).
10. P. K. Jain, X. H. Huang, I. H. El-Sayed, M. A. El-Sayed. *Acc. Chem. Res.* **41**, 1578 (2008).
11. C. J. Murphy, A. M. Gole, J. W. Stone, P. N. Sisco, A. M. Alkilany, E. C. Goldsmith, S. C. Baxter. *Acc. Chem. Res.* **41**, 1721 (2008).
12. A. M. Gobin, M. H. Lee, N. J. Halas, W. D. James, R. A. Drezek, J. L. West. *Nano Lett.* **7**, 1929 (2007).
13. J. C. Ostrowski, A. Mikhailovsky, D. A. Bussian, M. A. Summers, S. K. Buratto, G. C. Bazan. *Adv. Funct. Mater.* **16**, 1221 (2006).
14. R. Toftegaard, J. Arnbjerg, K. Daasbjerg, P. R. Ogilby, A. Dmitriev, D. S. Sutherland, L. Poulsen. *Angew. Chem., Int. Ed.* **47**, 6025 (2008).
15. J. R. Lakowicz, K. Ray, M. Chowdhury, H. Szmacinski, Y. Fu, J. Zhang, K. Nowaczyk. *Analyst* **133**, 1308 (2008).
16. A. Kinkhabwala, Z. F. Yu, S. H. Fan, Y. Avlasevich, K. Mullen, W. E. Moerner. *Nat. Photonics* **3**, 654 (2009).
17. P. R. Ogilby. *Chem. Soc. Rev.* **39**, 3181 (2010).
18. C. Schweitzer, R. Schmidt. *Chem. Rev.* **103**, 1685 (2003).
19. P. R. Ogilby. *Acc. Chem. Res.* **32**, 512 (1999).
20. J. W. Snyder, E. Skovsen, J. D. C. Lambert, L. Poulsen, P. R. Ogilby. *Phys. Chem. Chem. Phys.* **8**, 4280 (2006).
21. J. W. Snyder, I. Zebger, Z. Gao, L. Poulsen, P. K. Frederiksen, E. Skovsen, S. P. McIlroy, M. Klinger, L. K. Andersen, P. R. Ogilby. *Acc. Chem. Res.* **37**, 894 (2004).
22. J. P. Camden, J. A. Dieringer, J. Zhao, R. P. Van Duyne. *Acc. Chem. Res.* **41**, 1653 (2008).
23. A. Hartstein, J. R. Kirtley, J. C. Tsang. *Phys. Rev. Lett.* **45**, 201 (1980).

24. P. J. G. Goulet, R. F. Aroca. In *Radiative Decay Engineering*, C. D. Geddes, J. R. Lakowicz (Eds.), pp. 223–247, Springer, New York (2005).
25. J. R. Lakowicz, Y. Shen, S. D'Auria, J. Malicka, J. Fang, Z. Gryczynski, I. Gryczynski. *Anal. Biochem.* **301**, 261 (2002).
26. S. J. Oldenburg, R. D. Averitt, S. L. Westcott, N. J. Halas. *Chem. Phys. Lett.* **288**, 243 (1998).
27. C. J. Murphy, T. K. Sau, A. M. Gole, C. J. Orendorff, J. Gao, L. Gou, S. E. Hunyadi, T. Li. *J. Phys. Chem. B* **109**, 13857 (2005).
28. B. Nikoobakht, M. A. El-Sayed. *Chem. Mater.* **15**, 1957 (2003).
29. J. Pérez-Juste, I. Pastoriza-Santos, L. M. Liz-Marzán, P. Mulvaney. *Coord. Chem. Rev.* **249**, 1870 (2005).
30. S. A. Maier, H. A. Atwater. *J. Appl. Phys.* **98**, 011101 (2005).
31. G. A. F. W. L. Mie. *Ann. Phys.* **330**, 377 (1908).
32. H. Fredriksson, Y. Alaverdyan, A. Dmitriev, C. Langhammer, D. S. Sutherland, M. Zäch, B. Kasemo. *Adv. Mater.* **19**, 4297 (2007).
33. J. Aizpurua, P. Hanarp, D. S. Sutherland, M. Käll, G. W. Bryant, F. J. G. de Abajo. *Phys. Rev. Lett.* **90**, 057401 (2003).
34. S. Eustis, M. A. El-Sayed. *J. Appl. Phys.* **100**, 18243 (2006).
35. T. Härtling, Y. Alaverdyan, M. T. Wenzel, R. Kullock, M. Käll, L. M. Eng. *J. Phys. Chem. C* **112**, 4920 (2008).
36. K. Aslan, M. Wu, J. R. Lakowicz, C. D. Geddes. *J. Am. Chem. Soc.* **129**, 1524 (2007).
37. K. B. Male, J. J. Li, C. C. Bun, S. C. Ng, J. H. T. Luong. *J. Phys. Chem. C* **112**, 443 (2008).
38. F. Tam, G. P. Goodrich, B. R. Johnson, N. J. Halas. *Nano Lett.* **7**, 496 (2007).
39. K. Aslan, S. N. Malyn, C. D. Geddes. *J. Fluoresc.* **17**, 7 (2007).
40. S. L. Pan, L. J. Rothberg. *J. Am. Chem. Soc.* **127**, 6087 (2005).
41. Y. X. Zhang, K. Aslan, M. J. R. Previte, S. N. Malyn, C. D. Geddes. *J. Phys. Chem. B* **110**, 25108 (2006).
42. Y. Zhang, A. Dragan, C. D. Geddes. *J. Phys. Chem. C* **113**, 15811 (2009).
43. K. Aslan, M. Wu, J. R. Lakowicz, C. D. Geddes. *J. Fluoresc.* **17**, 127 (2007).
44. Y. Chen, K. Munechika, D. S. Ginger. *Nano Lett.* **7**, 690 (2007).
45. C. Langhammer, Z. Yuan, I. Zoric, B. Kasemo. *Nano Lett.* **6**, 833 (2006).
46. J. R. Lakowicz. *Anal. Biochem.* **337**, 171 (2005).
47. N. Ganesh, W. Zhang, P. C. Mathias, E. Chow, J. A. N. T. Soares, V. Malyarchuk, A. D. Smith, B. T. Cunningham. *Nat. Nanotechnol.* **2**, 515 (2007).
48. H. Cong, R. Toftegaard, J. Arnbjerg, P. R. Ogilby. *Langmuir* **26**, 4188 (2010).
49. R. D. Scurlock, S. Nonell, S. E. Braslavsky, P. R. Ogilby. *J. Phys. Chem.* **99**, 3521 (1995).
50. B. F. Minaev, S. Lunell, G. I. Kobzev. *J. Mol. Struct. (Theochem.)* **284**, 1 (1993).
51. Y. Zhang, K. Aslan, M. J. R. Previte, C. D. Geddes. *Proc. Natl. Acad. Sci. USA* **105**, 1798 (2008).
52. P. Hanarp, M. Käll, D. S. Sutherland. *J. Phys. Chem. B* **107**, 5768 (2003).
53. W. Huang, W. Qian, P. K. Jain, M. A. El-Sayed. *Nano Lett.* **7**, 3227 (2007).
54. B. M. Reinhard, M. Siu, H. Agarwal, A. P. Alivisatos, J. Liphardt. *Nano Lett.* **5**, 2246 (2005).
55. S.-C. Yang, H. Kobori, C.-L. He, M.-H. Lin, H.-Y. Chen, C. Li, M. Kanehara, T. Teranishi, S. Gwo. *Nano Lett.* **10**, 632 (2010).
56. R. L. Clough, M. P. Dillon, K. K. Iu, P. R. Ogilby. *Macromolecules* **22**, 3620 (1989).
57. R. D. Scurlock, D. O. Mártire, P. R. Ogilby, V. L. Taylor, R. L. Clough. *Macromolecules* **27**, 4787 (1994).
58. R. Hillenbrand, F. Keilmann, P. Hanarp, D. S. Sutherland, J. Aizpurua. *Appl. Phys. Lett.* **83**, 368 (2003).
59. A. Dmitriev, T. Pakizeh, M. Käll, D. S. Sutherland. *Small* **3**, 294 (2007).
60. E. Prodan, C. Radloff, N. J. Halas, P. Nordlander. *Science* **302**, 419 (2003).
61. T. D. Poulsen, P. R. Ogilby, K. V. Mikkelsen. *J. Phys. Chem. A* **102**, 9829 (1998).

62. L. K. Andersen, P. R. Ogilby. *J. Phys. Chem. A* **106**, 11064 (2002).
63. M. Hild, R. Schmidt. *J. Phys. Chem. A* **103**, 6091 (1999).
64. R. D. Scurlock, P. R. Ogilby. *J. Phys. Chem.* **91**, 4599 (1987).
65. M. J. Paterson, O. Christiansen, F. Jensen, P. R. Ogilby. *Photochem. Photobiol.* **82**, 1136 (2006).

